Check for updates

Electrochemical fabrication of FeS$_x$ films with high catalytic activity for oxygen evolution

Wenbin Wang, [ID] [a] Ruidong Xu,*[ab] Bohao Yu, [ID] [a] Xuanbin Wang[a] and Suyang Feng[a]

Electrochemical decomposition of water to produce oxygen (O$_2$) and hydrogen (H$_2$) through an anodic oxygen evolution reaction (OER) and a cathodic hydrogen evolution reaction (HER) is a promising green method for sustainable energy supply. Here, we demonstrate that cauliflower-like S-doped iron microsphere films are materials that can efficiently decompose water as an electrocatalyst for the oxygen evolution reaction. FeS$_x$ films are prepared by a simple one-step electrodeposition method and directly grow on copper foam from a deep eutectic solvent, ethaline (mixture of choline chloride and ethylene glycol), as a durable and highly efficient catalyst for the OER in 1.0 M KOH. The prepared FeS$_x$/CF, as an oxygen-evolving anode, shows remarkable catalytic performance toward the OER with a moderate Tafel slope of 105 mV dec^{-1}, and require an overpotential of only 340 mV to drive a geometrical catalytic current density of 10 mA cm^{-2}. In addition, this catalyst also demonstrates strong long-term electrochemical durability. This study provides a simple synthesis route for practical applications of limited transition metal nano catalysts.

1. Introduction

Over the past decades, as the world's population has grown and living standards have changed, energy has gained widespread attention as a fundamental driver.[1,2] In recent years, researchers have attempted to achieve sustainable development by developing new energy sources and utilizing renewable energy sources. Solar energy, wind energy, tidal energy, geothermal energy and other energy sources are expected to play an important role in the future development of human society. Affected by regional differences and intermittent supply, however, they are difficult to use on a large scale.[3] To solve the energy and environmental problems, efficient and green energy conversion and storage devices, such as fuel cells,[4] metal-air batteries[5] and electrolytic water,[6] have recently received widespread attention. Among them, electrolytic water is an energy conversion device that converts electric energy into hydrogen energy.[7] The electrolytic water reaction is carried out in an electrolytic cell. Under the action of direct current and catalyst, the water generates hydrogen and oxygen through electrochemical reaction on the electrode.[8] The cathode reacts with hydrogen evolution catalyst to produce hydrogen (HER), and the anode reacts with oxygen evolution catalyst to produce oxygen (OER). The oxygen release reaction has a slow kinetics (High Overpotential). Therefore, OER can be performed in any

medium, at room temperature (293 K), OER has a thermodynamic potential of 1.23 V *vs.* RHE.[9] However, in order to accelerate the catalytic reaction, a potential higher than the thermodynamic potential must be applied, which will lead to the consumption of excess energy and reduce the conversion frequency.[10–15] This extra potential (also called an overpotential) η mainly have intrinsic reactive activation barrier and some other resistances, such as solution resistance and contact resistance.[16] Therefore, it is urgent to develop OER catalysts with high catalytic performance and cost performance.

In recent years, although most non-expensive HER and OER electrocatalysts are based on crystalline compounds, an increasing number of amorphous materials have become more effective electrocatalysts than their crystalline counterparts, mainly including amorphous metal sulfides (*e.g.*, MoS$_x$ and CoS$_x$) for HER[17–20] and amorphous metal oxides (*e.g.*, MO$_x$, M = Fe, Co, and Ni) for OER.[21–25] Although some progress has been made in the study of strategies and catalytic properties for the synthesis of amorphous catalytic materials, fine design of microstructure of new amorphous materials and a deep understanding of their catalytic mechanism are necessary, which it is hoped that the newly developed materials will be efficient for HER and OER. To this end, we prepared a copper based material, which is composed of a high conductivity carrier with high surface area and a large amount of activity. We prepared cauliflower-like FeS$_x$ microsphere films using choline chloride (ChCl)–ethylene glycol (EG)-based deep eutectic solvent (ethaline) as high-performance OER catalyst using a simple potentiostatic electrodeposition method, with no template required.[17,26–28] Compared with water molecular

[a]Faculty of Metallurgical and Energy Engineering, Kunming University of Science and Technology, Kunming 650093, China. E-mail: 2545845040@qq.com

[b]State Key Laboratory of Complex Nonferrous Metal Resources Clean Utilization, Kunming 650093, China

solutions, the solvent properties of ethaline can provide a favorable chemical environment for producing nanostructured materials with high catalytic activity.[29]

In this paper, we report a simple and efficient method for preparing self-supporting FeS_x microsphere films grown directly on copper foam (labeled as FeS_x/CF), which is a highly durable and efficient catalyst for OER in alkaline media. The system without precious metal has unprecedented electrocatalytic activity of water oxidation and low potential stability under various conditions.[30]

2.   Experimental section

2.1   Chemicals and materials

Laboratory equipment and chemicals include ethylene glycol (EG, 99%), choline chloride (ChCl, 99%), ferric chloride hexahydrate ($FeCl_3 \cdot 6H_2O$, 98%), thiourea (CH_4N_2S, 99%), potassium hydroxide (KOH, 95%) are purchased from Aladdin Ltd. (Shanghai, China) and used as received. The deep eutectic solvent ethaline is synthesized by stirring the EG and ChCl together with a molar ratio of 1 : 2 at 353 K until a homogeneous liquid mixture is obtained.[31]

2.2   Electrochemical preparation of FeS_x/CF films

The CHI760D electrochemical workstation is the main equipment. 400 mM $FeCl_3 \cdot 6H_2O$ and 10 mM thiourea are weighed and placed in 40 ml eutectic solvent and stirred at 333 K. The FeS_x/CF electrodeposition is carried out in a standard three-electrode system, and s-doped iron films are prepared by one-step potentiostatic deposition. Among them, copper foam (the thickness of 1 mm, purity > 99.99%, 2.3 cm^2) is used as the working electrode, silver wire and platinum column are used as the reference electrode and the counter electrode, respectively. Before each deposition, the copper foam is ultrasonically cleaned in 1% HCl for 10 min, then in anhydrous ethanol for 10 min, ished with distilled water, and finally dried. The electrodeposition is carried out at a fixed potential of −0.95 V vs. Ag wire with various charge densities. After deposition, the samples are ished with anhydrous ethanol and deionized water successively and dried with air for further characterization.

2.3   Characterization

The morphology and element composition of the deposited samples are characterized by field emission scanning electron microscopy (SEM, Nove NanoSEM 450) equipped with energy dispersive X-ray (EDS) system. X-ray diffraction (XRD) patterns are recorded on a D/max 2200 X-ray diffractometer (XRD, Cu Kα radiation). X-ray photoelectron spectroscopy (XPS) analysis was detected on a PHI 5500 X-ray photoelectron spectroscope.

2.4   Electrochemical test

Electrocatalytic experiments are performed using linear sweep voltammetry (LSV), cyclic voltammetry (CV), and electrochemical impedance spectroscopy (EIS) and chronoamperometry. All measurements are performed at ambient temperature in a CHI760D electrochemical workstation with a 50 mL electrolyte (1.0 M KOH). This experiment FeS_x/CF, Hg/HgO and platinum column are respectively used as the working electrode, reference electrode and counter electrode. All the deposited samples were activated prior to any measurements as reported previously. All potentials, measured against a Hg/HgO electrode, are converted to the potential versus the reversible hydrogen electrode (RHE) according to E (vs. RHE) = E (vs. Hg/HgO) + 0.096 + 0.0591 pH. LSV is measured at the scanning rate of 5 mV s^{-1} in 1.0 M KOH. Electrochemical impedance spectroscopy measurements are performed at 0.75 V (vs. RHE) at the same configuration from 100 000 KHz to 0.1 Hz. Electrochemical two-layer capacitances are measured to determine the surface activity areas of the deposited products. For each sample, CV curves in the non-faraday voltage range (0.62–0.72 V vs. RHE) at various scan rates ranges from 5 to 200 mV^{-1}. The rough stability of the electrocatalyst prepared for FeS_x/CF is measured for 6000 scans by continuous cycle operation (1.0 to 1.7 V vs. RHE for the OER, 100 mV^{-1}). The timing-current diagram is measured to assess the durability of the catalyst at 1.50 V in 1.0 M KOH solution.

3.   Results and discussion

Under the condition of 293 K, the voltage of electrolysis at constant potential is −0.95 V (vs. Ag wire), and the electrodeposition times are 35 min, 45 min, 55 min and 65 min, respectively. The electrochemical activity for oxygen evolution reaction (OER) was measured by linear sweep voltammetry (LSV) with catalysts obtained at different deposition times. All electrochemical tests were carried out in a solution of 1 M KOH electrolyte, and the LSV shows a scanning rate of 5 mV s^{-1}. After the electrodeposition of the copper foam (CF), it is obvious that the fuchsia CF turns black. Fig. 1 shows the polarization curve of electrocatalytic water oxidation of catalyst FeS_x/CF prepared at different electrodeposition times. Comparison of the LSV
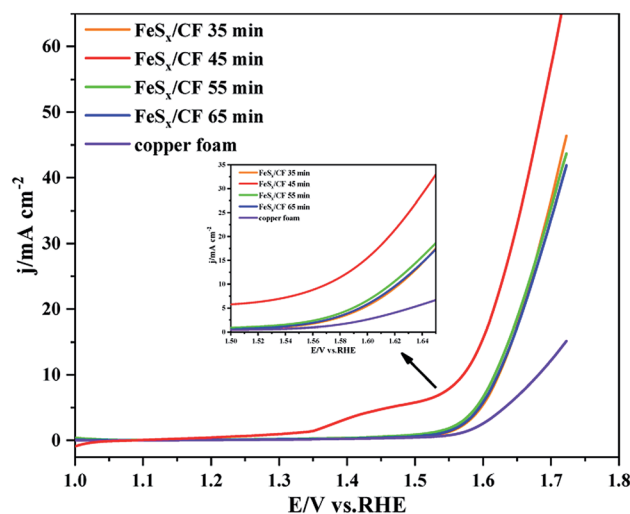

Fig. 1 Electrocatalytic water oxidation polarization curves of the FeS_x/CF electrodes fabricated with different electrodeposition time to create the surface FeS_x species.

diagram in Fig. 1 shows that catalyst FeS_x/CF in 1 M KOH solution for electrocatalytic OER, produced by the catalytic current density, increased with the increase of electrodeposition time, and show the trend of initial increase followed by a decrease. When the electrodeposition time increased from 35 min to 45 min, the electrocatalytic activity for OER increased gradually. When the electrodeposition time increased from 45 min to 65 min, electrocatalytic activity for OER gradually decreased. Therefore, it was confirmed that at electrodeposition time of 45 min, the catalytic current density is the maximum at the same voltage as when the obtained catalyst conducts electrocatalytic OER in 1 M KOH solution. In other words, the electrodeposition time of 45 min is the optimal electrodeposition time.

In this experiment, X-ray diffractometer (XRD) was used to analyse catalyst FeS_x/CF prepared with an electrodeposition time of 45 min. Fig. 2a presents the XRD patterns of pure Fe (blue line) and FeS_x (red line). Except for the strong signal from the Cu substrate, the XRD pattern for the as-prepared Fe/CF (blue line) matches well with the face-centred cubic Fe phase

(PDF#06–0696). Diffraction peaks of iron and copper also exist in the samples with added thiourea (red line). This indicates that the deposit containing thiourea in solution is amorphous. In contrast, the S-doped product shows a shift of the diffraction peaks towards lower angles compared with the pure Fe sample (inset in Fig. 2a).

The chemical compositions and surface states of the as-prepared sample were further identified by XPS, as shown in Fig. 2b–d. In the XPS survey, peaks in the full XPS spectrum indicate the existence of Cu, Fe, O, and C elements. The presence of O and C comes from surface attack of the deposited sample and trace solvent residues. XPS spectra of the Fe 2p and S 2p regions of the as-deposited sample are shown in Fig. 2c and d. The Fe 2p levels are split into $2p_{3/2}$ and $2p_{1/2}$ doublets owing to the spin–orbit coupling[32–34] (we only analyze Fe $2p_{3/2}$ in Fig. 2c). As seen from the XPS image, Fe $2p_{3/2}$ identified five splitting peaks, and the corresponding binding energies and combined states were 706.7 eV (FeS_2),[35] 708.2 eV (Fe_3O_4),[36] 709.4 eV (FeO),[37] 710.3 eV (FeS),[38] and 712.2 eV (FeS),[38] respectively. The two peaks at 708.2 eV and 709.4 eV were attributed to
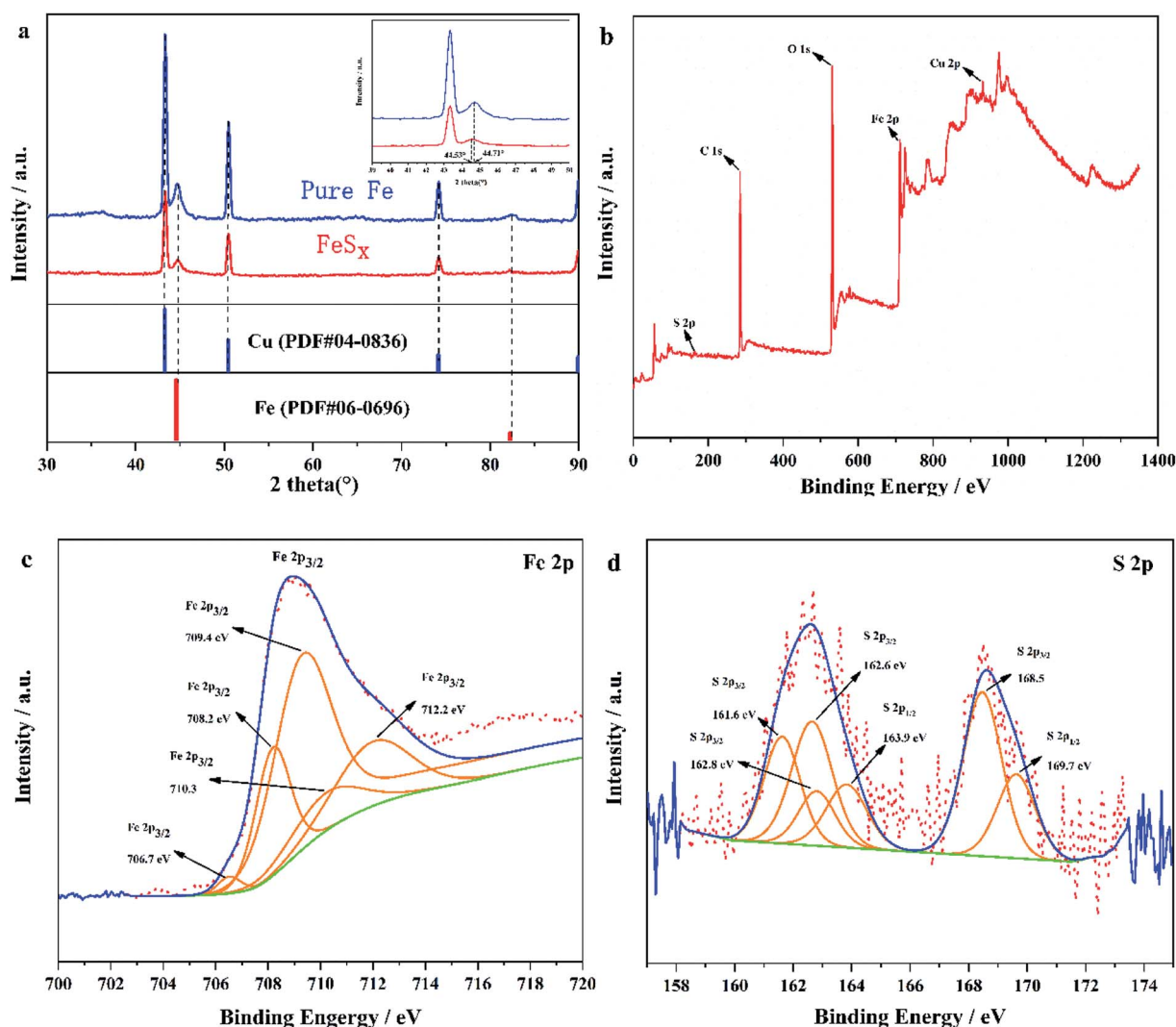

Fig. 2 (a) XRD pattern of the sample only consisting of FeS_x/CF. Comparison XPS surveys of FeS_x/CF (b) full survey, (c) Fe 2p and (d) S 2p.
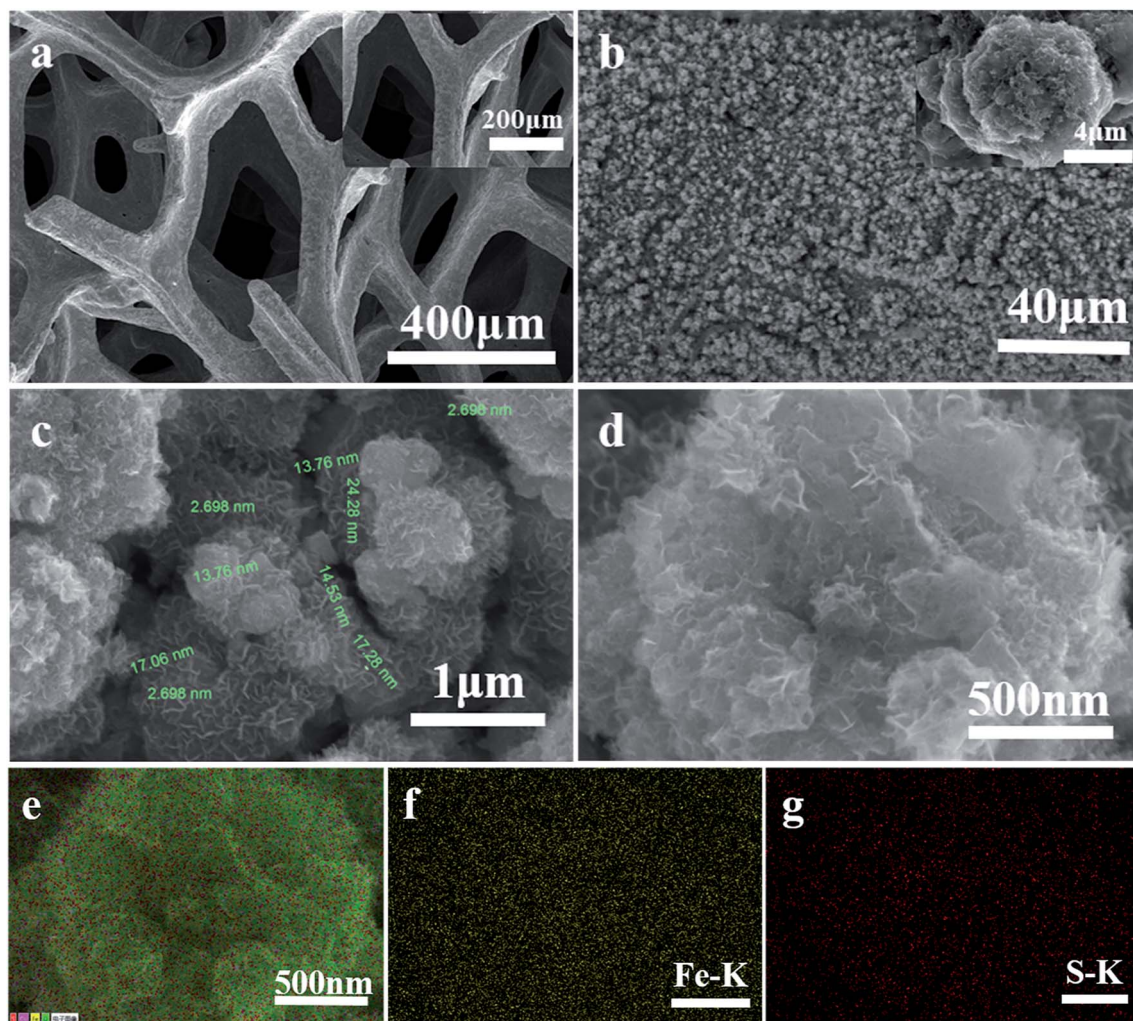
Fig. 3 (a) SEM image of copper foam surface. (b–d) The associated high magnification SEM image clearly shows that cauliflower-like FeS_x microsphere films is made up of many nanosheets. (e–g) The corresponding element mapping images of Fe and S, the scale bars are all 500 nm.

the oxidation of the sample surface. As oxidation is easy when FeS_2 encounters oxygen, and it can be seen from the XPS spectrum of S that SO_4^{2-} ions exist at the binding energy 168.5 eV (Fig. 2d). In the iron picture, the binding energy 712.2 eV is attributed to the partial oxidation of FeS_2 to $FeSO_4$.[38] In the S 2p region (Fig. 2d), the two groups of peak at 161.6 eV,
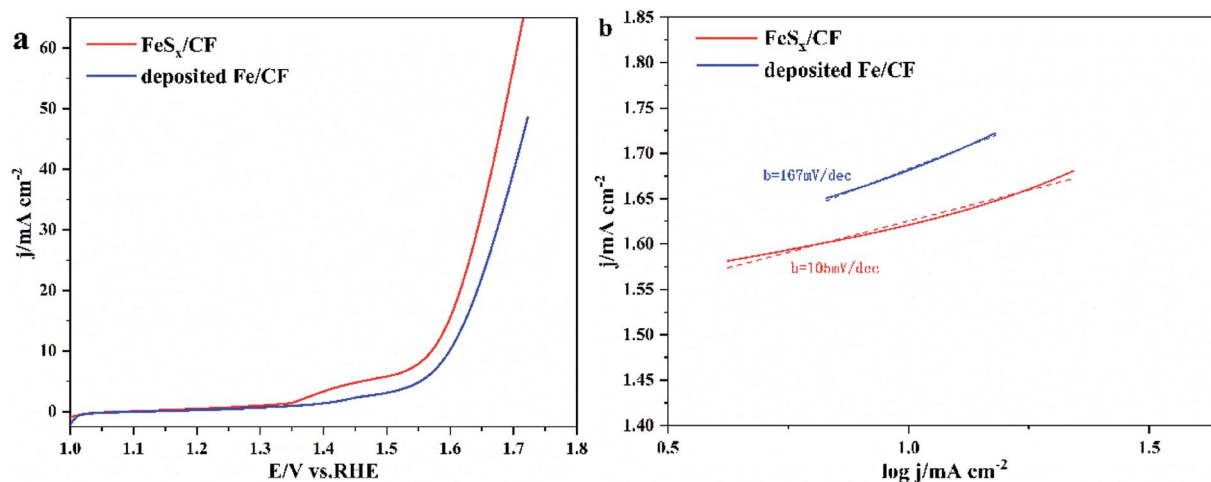

Fig. 4 (a) The polarization curves of FeS_x/CF and deposited Fe/CF with scanning rate of 5 mV s^{-1}. (b) Corresponding Tafel plots with linear fitting.

Table 1 Comparison of OER performance for FeS$_x$/CF and deposited Fe/CF with other nonnoble-metal OER catalysts under alkaline conditions

Catalyst	j (mA cm^{-2})	η (mV)	Electrolyte	Ref.
FeS$_x$/CF	10	340	1 M KOH	This work
Deposited Fe/CF	10	369	1 M KOH	This work
Fe(OH)$_3$: Cu(OH)$_2$/CF	10	365	1 M KOH	43
Co–CoO@3DHPG	10	410	1 M KOH	44
FeN$_x$/carbon	10	360	1 M KOH	45
NiS/NC	10	371	1 M KOH	46
2D CuO nanosheet bundles	10	350	1 M KOH	47

162.8 eV; and 162.6 eV, 163.9 eV belong to S 2p$_{3/2}$ and S 2p$_{1/2}$ respectively, which are related to the binding energy of S^{2-} and S$_2{}^{2-}$ ligands. The other peak at 168.3 eV is the binding energy of Fe–O–S, which is caused by surface oxidation in air.[39,40] Thus, it suggests that S doped enter into Fe. These results indicate that the FeS$_x$ obtained by electrodeposition has poor crystal form and may even be amorphous. It also means that the FeS$_x$ films in FeS$_x$/CF may consists of small clusters in which Fe is in the

FeS and FeS$_2$ states. The ratio of the atomic radius of Fe (atomic radius 117 pm) and S (atomic radius 104 pm)[41,42] is greater than 0.59, which further proves that S is doped into the lattice of Fe to form interstitial compounds. The interstitial compound can be called FeS$_x$.

Fig. 3a shows that the whole surface of the CF is bright and smooth. Fig. 3b shows that the whole surface of the CF is uniformly covered with cauliflower-like FeS$_x$ microsphere films
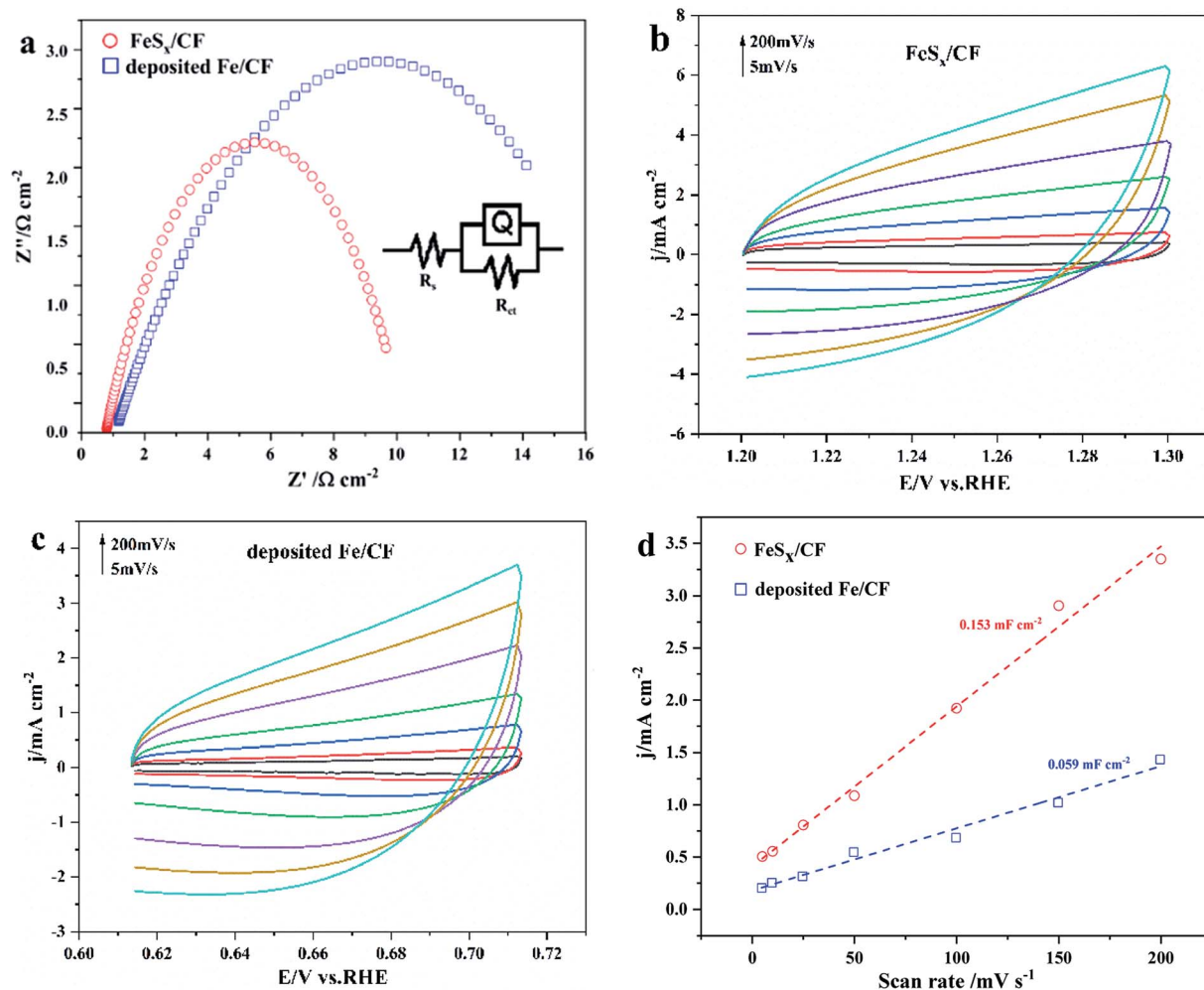

Fig. 5 (a) Nyquist plots of FeS$_x$/CF and deposited Fe/CF at 0.75 V (*vs.* RHE). (b and c) CV curves of FeS$_x$/CF and deposited Fe/CF catalyst in non-faraday voltage range (0.62–0.72 V *vs.* RHE). (d) The relationship between charging current density difference ($j_a − j_c$) and scanning rate is shown in the figure. The slope in the figure is twice that of C_{dl}.

(inset in Fig. 3b). The associated high magnification SEM image (Fig. 3c and d) clearly shows that the cauliflower-like FeS_x microsphere films is made up of many nanosheets. Meanwhile, samples of the catalyst FeS_x/CF with electrodeposition time of 45 min were characterized by element mapping analysis in SEM. In the element distribution diagrams of SEM, Fe and S are shown in Fig. 3c–e. It can be seen from Fig. 3d and e that Fe and S elements are evenly distributed on the entire sample surface.

The electrocatalytic activity of the prepared FeS_x/CF OER was assessed in 1.0 M KOH by steady-state LSV with a scan rate 5 mV s^{-1}. For comparison with the FeS_x/CF catalyst, pure Fe was deposited onto CF electrode by measurement of electrochemical properties. Fig. 4a shows the polarization curve compensation of these catalysts without iR. As expected, FeS_x/CF shows excellent OER activity, whereas the deposited Fe/CF exhibits poor OER activity and greater starting potential. The FeS_x/CF enables OER with high catalytic activity and relatively low starting potential (1.57 V). When the current density reaches 10 mA cm^{-2}, the overpotential of the sample in 1 M KOH

solution was 340 mV. This overpotential compares favourably with the behaviour of Cu-based OER electrocatalysts, except FeS_x/CF composites such as $Fe(OH)_3 : Cu(OH)_2$/CF ($\sim$365 mV),[43] Co–CoO@3DHPG ($\sim$410 mV),[44] FeN_x/carbon ($\sim$320 mV),[45] NiS/NC ($\sim$371 mV),[46] and 2D CuO nanosheet bundles ($\sim$350 mV),[47] etc. A more detailed comparison is given in Table 1. Fig. 4b shows the Tafel slopes for FeS_x/CF and deposited Fe/CF. The Tafel plots are fitted with the formula: $\eta = b \log j + a$ (where j is the current density and b is the Tafel slope). The Tafel slope of catalyst FeS_x/CF (105 mV dec^{-1}) is higher than that of deposited Fe/CF (167 mV dec^{-1}), implying more favorable catalytic kinetics on FeS_x/CF.

Electrochemical impedance spectroscopy (EIS) data (Fig. 5a) reveal that FeS_x/CF, with a much smaller semicircle radius compared with deposited Fe/CF, manifests the high conductivity of the as-prepared electrode, and lower polarization resistance (R_{ct}). Accordingly, FeS_x/CF has faster charge transfer and OER kinetics. These result show that the electrode dynamics mainly controls the charge transfer process, and the
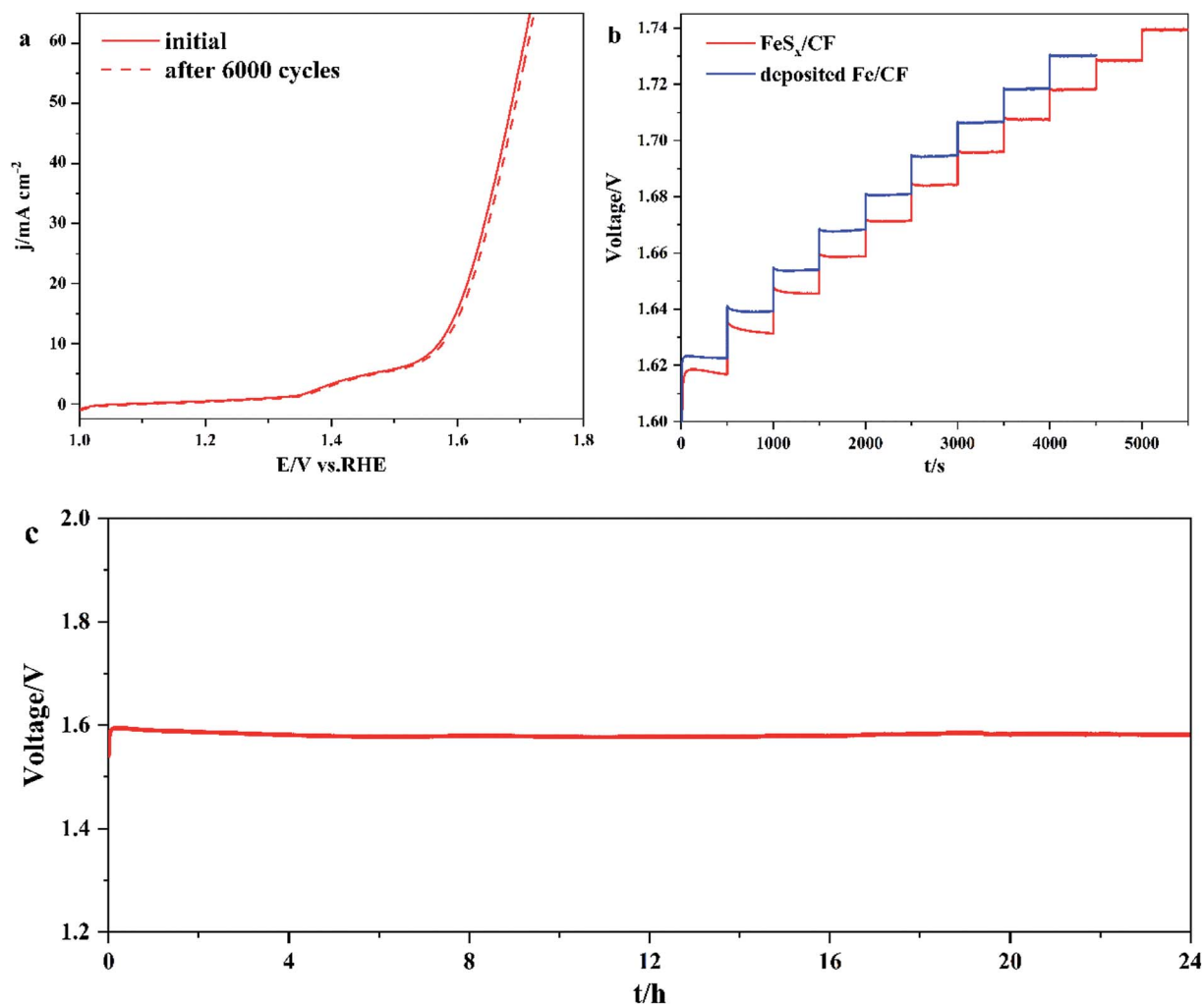

Fig. 6 (a) At the scanning rate of 100 mV s^{-1}, the polarization curve of FeS_x/CF before and after 6000 voltage sweeps between 1.0 V and 1.7 V vs. RHE. (b) Multistep chronopotentiometric curve for FeS_x/CF with current density ranging from 10 to 60 mA cm^{-2}, and the deposited Fe/CF with current density ranging from 10 to 50 mA cm^{-2}, without iR compensation. (c) Chronopotential curve recorded at constant current density of 10 mA cm^{-2}.

electrochemical system is approximated by the modified Randles circuit, as shown in the inset of Fig. 4a. The potential dependencies of the obtained data include solution resistance (R_s), charge-transfer resistance (R_{ct}), and constant-phase element related to the double-layer capacitance (CPE).[48]

The contribution of S-doping to the catalytic activity of these electrodes was evaluated, considering that the electrocatalytic activity for OER is highly dependent on their electrochemically active surface area (ECSA) and reaction active sites. CVs of catalyst FeS$_x$/CF and deposited Fe/CF samples were recorded at different scanning rates from 5 to 200 mV s^{-1} in the faradaic silent region (Fig. 5b and c). From the measured capacitances (Fig. 5d), the C_{dl} of porous FeS$_x$/CF and deposited Fe/CF are 0.153 mF cm^{-2} and 0.059 mF cm^{-2}, respectively, suggesting a much larger ECSA of the FeS$_x$/CF electrode, which is consistent with the LSV and EIS results. The findings suggest that the large ECSA generated by the structural characteristics of FeS$_x$/CF plays a crucial role in its high catalytic activity. The rough nanosheet structure not only leads to more effective exposure of catalytic activity sites, but also promotes rapid electron transfer and ion diffusion, thereby improving OER catalytic activity.

In order to obtain the stability of FeS$_x$/CF, CV scans were performed at 1.0 and 1.7 V vs. RHE for 6000 consecutive cycles with a scanning rate of 100 mV s^{-1}. The FeS$_x$/CF catalyst remained stable after thousands of cycles (Fig. 6a). To further prove stability, Fig. 6b shows a multistep chronopotentiometric curve for FeS$_x$/CF with current density ranging from 10 to 60 mA cm^{-2} (5 mA cm^{-2} per 500 s), and the deposited Fe/CF with current density ranging from 10 to 50 mA cm^{-2} (5 mA cm^{-2} per 500 s). In the range of 1.60–1.74 V, all steps remained unchanged for 500 s, which means that the FeS$_x$/CF electrode has higher conductivity, better mechanical strength, and better mass transfer than the Fe/CF electrode. For long-term electrolysis at a constant current density of 10 mA cm^{-2} (Fig. 6c), the FeS$_x$/CF exhibits strong electrochemical stability, maintaining its original OER activity for at least 24 h with negligible degradation. These results show that the FeS$_x$/CF electrode has a great potential in practical alkaline water electrolysis applications.

4. Conclusion

In summary, FeS$_x$ films is successfully prepared on copper foam by a simple electrodeposition method. The as prepared FeS$_x$/CF catalyst shows excellent electrocatalytic activity, durability and low overpotential. It is expected that FeS$_x$/CF hold great promise for developing a cheap electrode material for electrocatalytic OER. Notably, this electrode material has great potential for large-scale and low-cost oxygen production through water decomposition. Besides, the proposed simple electrodeposition method can use to prepare other transition metal based nanomaterials for application of electrochemical oxygen generation.

Conflicts of interest

There are no conflicts to declare.

Acknowledgements

References

1 B. Gates, The energy research imperative, *Science*, 2011, **334**(6058), 877.

2 S. Chu and A. Majumdar, Opportunities and challenges for a sustainable energy future, *Nature*, 2012, **488**(7411), 294–303.

3 Y.-G. Guo, J.-S. Hu and L.-J. Wan, Nanostructured Materials for Electrochemical Energy Conversion and Storage Devices, *Adv. Mater.*, 2008, **20**(15), 2878–2887.

4 O. Z. Sharaf and M. F. Orhan, An overview of fuel cell technology: Fundamentals and applications, *Renewable Sustainable Energy Rev.*, 2014, **32**, 810–853.

5 K. F. Blurton and A. F. Sammells, Metal/air batteries: their status and potential—a review, *J. Power Sources*, 1979, **4**(4), 263–279.

6 M. D. Symes and L. Cronin, Decoupling hydrogen and oxygen evolution during electrolytic water splitting using an electron-coupled-proton buffer, *Nat. Chem.*, 2013, **5**(5), 403.

7 M. Tanaka, Y. Nishiki, N. Hayamizu and N. Sakurai, Apparatus for producing electrolytic water, *US Pat.*, 6,235,186, 2001-5-22.

8 B. Conway, Electrochemical proton transfer and cathodic hydrogen evolution, *Sci. Prog.*, 1987, (1933-), 479–509.

9 J.-L. Tao and Y.-Q. Xiong, Hydrogen production from the decomposition of ethanol aqueous solution using glow discharge plasma electrolysis, *Acta Phys.-Chim. Sin.*, 2013, **29**(1), 205–211.

10 X. Sun, Y. Guo, C. Wu and Y. Xie, The hydric effect in inorganic nanomaterials for nanoelectronics and energy applications, *Adv. Mater.*, 2015, **27**(26), 3850–3867.

11 W. Lu, T. Liu, L. Xie, C. Tang, D. Liu, S. Hao, F. Qu, G. Du, Y. Ma and A. M. Asiri, In Situ Derived Co B Nanoarray: A High-Efficiency and Durable 3D Bifunctional Electrocatalyst for Overall Alkaline Water Splitting, *Small*, 2017, **13**(32), 1700805.

12 W. Zhu, R. Zhang, F. Qu, A. M. Asiri and X. Sun, Design and application of foams for electrocatalysis, *ChemCatChem*, 2017, **9**(10), 1721–1743.

13 X. Ren, R. Ge, Y. Zhang, D. Liu, D. Wu, X. Sun, B. Du and Q. Wei, Cobalt–borate nanowire array as a high-performance catalyst for oxygen evolution reaction in near-neutral media, *J. Mater. Chem. A*, 2017, **5**(16), 7291–7294.

14 Q. Liu, L. Xie, Z. Liu, G. Du, A. M. Asiri and X. Sun, A Zn-doped Ni$_3$S$_2$ nanosheet array as a high-performance electrochemical water oxidation catalyst in alkaline solution, *Chem. Commun.*, 2017, **53**(92), 12446–12449.

15 R. Xu, R. Wu, Y. Shi, J. Zhang and B. Zhang, Ni_3Se_2 nanoforest/Ni foam as a hydrophilic, metallic, and self-supported bifunctional electrocatalyst for both H_2 and O_2 generations, *Nano Energy*, 2016, **24**, 103–110.

16 L. Han, S. Dong and E. Wang, Transition-Metal (Co, Ni, and Fe)-Based Electrocatalysts for the Water Oxidation Reaction, *Adv. Mater.*, 2016, **28**(42), 9266–9291.

17 M. Gao, C. Yang, Q. Zhang, Y. Yu, Y. Hua, Y. Li and P. Dong, Electrochemical fabrication of porous Ni-Cu alloy nanosheets with high catalytic activity for hydrogen evolution, *Electrochim. Acta*, 2016, **215**, 609–616.

18 Y. Liu, Q. Li, R. Si, G. D. Li, W. Li, D. P. Liu, D. Wang, L. Sun, Y. Zhang and X. Zou, Coupling Sub-Nanometric Copper Clusters with Quasi-Amorphous Cobalt Sulfide Yields Efficient and Robust Electrocatalysts for Water Splitting Reaction, *Adv. Mater.*, 2017, **29**(13), 1606200.

19 P. D. Tran, T. V. Tran, M. Orio, S. Torelli, Q. D. Truong, K. Nayuki, Y. Sasaki, S. Y. Chiam, R. Yi and I. Honma, Coordination polymer structure and revisited hydrogen evolution catalytic mechanism for amorphous molybdenum sulfide, *Nat. Mater.*, 2016, **15**(6), 640.

20 J. Staszak-Jirkovský, C. D. Malliakas, P. P. Lopes, N. Danilovic, S. S. Kota, K.-C. Chang, B. Genorio, D. Strmcnik, V. R. Stamenkovic and M. G. Kanatzidis, Design of active and stable Co–Mo–S_x chalcogels as pH-universal catalysts for the hydrogen evolution reaction, *Nat. Mater.*, 2016, **15**(2), 197.

21 C. L. Farrow, D. K. Bediako, Y. Surendranath, D. G. Nocera and S. J. Billinge, Intermediate-range structure of self-assembled cobalt-based oxygen-evolving catalyst, *J. Am. Chem. Soc.*, 2013, **135**(17), 6403–6406.

22 X. L. Hu, S. Piccinin, A. Laio and S. Fabris, Atomistic structure of cobalt-phosphate nanoparticles for catalytic water oxidation, *ACS Nano*, 2012, **6**(12), 10497–10504.

23 D. A. Salvatore, K. E. Dettelbach, J. R. Hudkins and C. P. Berlinguette, Near-infrared–driven decomposition of metal precursors yields amorphous electrocatalytic films, *Sci. Adv.*, 2015, **1**(2), e1400215.

24 R. D. Smith, M. S. Prévot, R. D. Fagan, Z. Zhang, P. A. Sedach, M. K. J. Siu, S. Trudel and C. P. Berlinguette, Photochemical route for accessing amorphous metal oxide materials for water oxidation catalysis, *Science*, 2013, **340**(6128), 60–63.

25 J. Zhu, F. Lambert, C. Policar, F. Mavré and B. Limoges, Fast magnetically driven electrodeposition of amorphous metal oxide water oxidation catalysts from carbon-coated metallic nanoparticles, *J. Mater. Chem. A*, 2015, **3**(31), 16190–16197.

26 M. Gao, C. Yang, Q. Zhang, J. Zeng, X. Li, Y. Hua, C. Xu and P. Dong, Facile electrochemical preparation of self-supported porous Ni–Mo alloy microsphere films as efficient bifunctional electrocatalysts for water splitting, *J. Mater. Chem. A*, 2017, **5**(12), 5797–5805.

27 C. Yang, Q. Zhang and A. P. Abbott, Facile fabrication of nickel nanostructures on a copper-based template *via* a galvanic replacement reaction in a deep eutectic solvent, *Electrochem. Commun.*, 2016, **70**, 60–64.

28 J. Zeng, M. Gao, Q. Zhang, C. Yang, X. Li, W. Yang, Y. Hua, C. Xu and Y. Li, Facile electrodeposition of cauliflower-like S-doped nickel microsphere films as highly active catalysts for electrochemical hydrogen evolution, *J. Mater. Chem. A*, 2017, **5**(29), 15056–15064.

29 D. V. Wagle, H. Zhao and G. A. Baker, Deep eutectic solvents: sustainable media for nanoscale and functional materials, *Acc. Chem. Res.*, 2014, **47**(8), 2299–2308.

30 T. N. Huan, G. Rousse, S. Zanna, I. T. Lucas, X. Xu, N. Menguy, V. Mougel and M. Fontecave, A dendritic nanostructured copper oxide electrocatalyst for the oxygen evolution reaction, *Angew. Chem., Int. Ed.*, 2017, **56**(17), 4792–4796.

31 A. P. Abbott, G. Capper, D. L. Davies, K. J. McKenzie and S. U. Obi, Solubility of metal oxides in deep eutectic solvents based on choline chloride, *J. Chem. Eng. Data*, 2006, **51**(4), 1280–1282.

32 N. Cheng, Q. Liu, A. M. Asiri, W. Xing and X. Sun, A Fe-doped Ni_3S_2 particle film as a high-efficiency robust oxygen evolution electrode with very high current density, *J. Mater. Chem. A*, 2015, **3**(46), 23207–23212.

33 M. Sun, X.-R. Ru and L.-F. Zhai, In-situ fabrication of supported iron oxides from synthetic acid mine drainage: high catalytic activities and good stabilities towards electro-Fenton reaction, *Appl. Catal., B*, 2015, **165**, 103–110.

34 Y. Qiu, J. Yu, W. Wu, J. Yin and X. Bai, Fe–N/C nanofiber electrocatalysts with improved activity and stability for oxygen reduction in alkaline and acid solutions, *J. Solid State Electrochem.*, 2013, **17**(3), 565–573.

35 S. Nakamura and A. Yamamoto, Electrodeposition of pyrite (FeS_2) thin films for photovoltaic cells, *Sol. Energy Mater. Sol. Cells*, 2001, **65**(1–4), 79–85.

36 D. Wilson and M. Langell, XPS analysis of oleylamine/oleic acid capped Fe_3O_4 nanoparticles as a function of temperature, *Appl. Surf. Sci.*, 2014, **303**, 6–13.

37 K. Prince, M. Matteucci, K. Kuepper, S. Chiuzbaian, S. Bartkowski and M. Neumann, Core-level spectroscopic study of FeO and FeS_2, *Phys. Rev. B*, 2005, **71**(8), 085102.

38 M. Descostes, F. Mercier, N. Thromat, C. Beaucaire and M. Gautier-Soyer, Use of XPS in the determination of chemical environment and oxidation state of iron and sulfur samples: constitution of a data basis in binding energies for Fe and S reference compounds and applications to the evidence of surface species of an oxidized pyrite in a carbonate medium, *Appl. Surf. Sci.*, 2000, **165**(4), 288–302.

39 H. Khani and D. O. Wipf, Iron oxide nanosheets and pulse-electrodeposited Ni–Co–S nanoflake arrays for high-performance charge storage, *ACS Appl. Mater. Interfaces*, 2017, **9**(8), 6967–6978.

40 N. Yang, C. Tang, K. Wang, G. Du, A. M. Asiri and X. Sun, Iron-doped nickel disulfide nanoarray: A highly efficient and stable electrocatalyst for water splitting, *Nano Res.*, 2016, **9**(11), 3346–3354.

41 D. K. Lonsdale, *International tables for X-ray crystallography*, Kynoch Press, 1968.

42 O. Senkov and D. Miracle, Effect of the atomic size distribution on glass forming ability of amorphous metallic alloys, *Mater. Res. Bull.*, 2001, **36**(12), 2183–2198.

43 C.-C. Hou, C.-J. Wang, Q.-Q. Chen, X.-J. Lv, W.-F. Fu and Y. Chen, Rapid synthesis of ultralong $Fe(OH)_3 : Cu(OH)_2$ core–shell nanowires self-supported on copper foam as a highly efficient 3D electrode for water oxidation, *Chem. Commun.*, 2016, **52**(100), 14470–14473.

44 N. Ullah, W. Zhao, X. Lu, C. J. Oluigbo, S. A. Shah, M. Zhang, J. Xie and Y. Xu, In situ growth of M-MO (M = Ni, Co) in 3D graphene as a competent bifunctional electrocatalyst for OER and HER, *Electrochim. Acta*, 2019, **298**, 163–171.

45 J. Ding, P. Wang, S. Ji, H. Wang, V. Linkov and R. Wang, N-doped mesoporous FeNx/carbon as ORR and OER bifunctional electrocatalyst for rechargeable zinc-air batteries, *Electrochim. Acta*, 2019, **296**, 653–661.

46 J. Ding, S. Ji, H. Wang, H. Gai, F. Liu, V. Linkov and R. Wang, Mesoporous nickel-sulfide/nickel/N-doped carbon as HER and OER bifunctional electrocatalyst for water electrolysis, *Int. J. Hydrogen Energy*, 2019, **44**(5), 2832–2840.

47 S. M. Pawar, B. S. Pawar, B. Hou, J. Kim, A. T. A. Ahmed, H. S. Chavan, Y. Jo, S. Cho, A. I. Inamdar and J. L. Gunjakar, Self-assembled two-dimensional copper oxide nanosheet bundles as an efficient oxygen evolution reaction (OER) electrocatalyst for water splitting applications, *J. Mater. Chem. A*, 2017, **5**(25), 12747–12751.

48 C. C. McCrory, S. Jung, J. C. Peters and T. F. Jaramillo, Benchmarking heterogeneous electrocatalysts for the oxygen evolution reaction, *J. Am. Chem. Soc.*, 2013, **135**(45), 16977–16987.